Deriving Arctic Cloud Microphysics at Barrow, Alaska: Algorithms, Results, and Radiative Closure

MATTHEW D. SHUPE,* DAVID D. TURNER,+ ALEXANDER ZWINK,# MANDANA M. THIEMAN,@ ELI J. MLAWER,& AND TIMOTHY SHIPPERT**

* *Cooperative Institute for Research in Environmental Sciences, and NOAA/Earth System Research Laboratory, Boulder, Colorado*
+ *NOAA/National Severe Storms Laboratory, Norman, Oklahoma*
# *University of Oklahoma, Norman, Oklahoma*
@ *Science Systems and Applications, Inc., Hampton, Virginia*
& *Atmospheric and Environmental Research, Lexington, Massachusetts*
** *Pacific Northwest National Laboratory, Richland, Washington*

(Manuscript received 20 February 2015, in final form 21 April 2015)

ABSTRACT

Cloud phase and microphysical properties control the radiative effects of clouds in the climate system and are therefore crucial to characterize in a variety of conditions and locations. An Arctic-specific, ground-based, multisensor cloud retrieval system is described here and applied to 2 yr of observations from Barrow, Alaska. Over these 2 yr, clouds occurred 75% of the time, with cloud ice and liquid each occurring nearly 60% of the time. Liquid water occurred at least 25% of the time, even in winter, and existed up to heights of 8 km. The vertically integrated mass of liquid was typically larger than that of ice. While it is generally difficult to evaluate the overall uncertainty of a comprehensive cloud retrieval system of this type, radiative flux closure analyses were performed in which flux calculations using the derived microphysical properties were compared with measurements at the surface and the top of the atmosphere. Radiative closure biases were generally smaller for cloudy scenes relative to clear skies, while the variability of flux closure results was only moderately larger than under clear skies. The best closure at the surface was obtained for liquid-containing clouds. Radiative closure results were compared with those based on a similar, yet simpler, cloud retrieval system. These comparisons demonstrated the importance of accurate cloud-phase and cloud-type classification, and specifically the identification of liquid water, for determining radiative fluxes. Enhanced retrievals of liquid water path for thin clouds were also shown to improve radiative flux calculations.

1. Introduction

Clouds have first-order effects on global radiation and precipitation. They cover nearly 70% of the globe at any given time (Stubenrauch et al. 2013) and are a significant mechanism through which spatial and temporal variability manifest in both weather and climate. In part because they occur under such a wide variety of conditions and compositions, clouds have been a challenge to model (Walsh et al. 2009; Klein et al. 2009; de Boer et al. 2012). The clear importance of clouds and current difficulties in modeling them demonstrate the present need for more cloud observations with which to develop and constrain models and study global climate processes. One key method for providing needed cloud observations is the use of intensive ground-based observatories, which hold the potential to measure cloud properties in all conditions and over long periods of time.

Many ground-based remote-sensor retrieval algorithms have been developed over the past few decades to quantify cloud microphysical properties. Because of design specifications and/or limitations of instruments and measurements, most retrievals are developed for application in specific conditions and cloud types. While the results of individual methods and related studies have greatly improved our knowledge of many aspects of cloudiness, there is a need for broadly applicable algorithms to operationally characterize all cloud types observed over multiple sites. Such algorithms must be designed to coordinate and capitalize on the strengths of multiple synergistic instruments.

Corresponding author address: Matthew D. Shupe, R/PSD3, 325 Broadway, Boulder, CO 80305.
E-mail: matthew.shupe@noaa.gov

DOI: 10.1175/JAMC-D-15-0054.1

TABLE 1. Specific measurements used in the ST cloud property retrieval system. Note that the ceilometer is an extra constraint on the system and is generally redundant for a lidar.

Instrument	Measurements
Millimeter Cloud Radar (MMCR), 35 GHz	Reflectivity (Z_e), mean Doppler velocity (V_D), Doppler spectrum width (W_D), cloud-top height (z_{top})
Micropulse lidar (MPL), 532 nm	Backscatter (β), depolarization ratio (δ), cloud-base height (z_{base})
Atmospheric Emitted Radiance Interferometer (AERI)	Radiances at multiple infrared microwindows between 8 and 19 μm
Microwave Radiometer (MWR), 23–31 GHz	Brightness temperatures (T_B)
Ceilometer	Cloud-base height (z_{base})
Interpolated radiosonde and/or merged sonde product	Temperature profiles [$T(z)$]

Recently, a number of ground-based cloud retrieval suites have been under development at various global locations including three sites in Western Europe (Illingworth et al. 2007), the Southern Great Plains site in the central United States (Mace et al. 2006a; Dunn et al. 2011), and a site in the tropical western Pacific Ocean (Mather et al. 2007). Long, continuous cloud products derived from surface-based measurements have been used to characterize cloud properties (Shupe et al. 2005; Mace et al. 2006a), compute atmospheric radiative heating rate profiles (Mace et al. 2006b; Mather et al. 2007), evaluate model simulations (Illingworth et al. 2007; de Boer et al. 2012), and compare with satellite measurements (Dong et al. 2002; Mace et al. 2005).

Here, we outline a cloud microphysics retrieval system that has been specifically designed for application at Arctic atmospheric observatories. The algorithm combines measurements from radiosondes, lidar, radar, microwave radiometer, and infrared radiometer within a framework that consists of multiple ground-based remote-sensor retrieval methods to produce estimates of cloud water content and hydrometeor size for both liquid and ice phases. The strength of the algorithm lies in the instrument and retrieval synergy. For example, while infrared measurements are accurate at determining cloud properties for optically thin clouds, they provide little information for thick clouds. Cloud radar provides information on all observed clouds, yet struggles to distinguish and characterize both liquid and ice phases. Microwave radiometer measurements give a good estimate of the total amount of liquid water above a certain threshold, but cannot distribute that liquid in the vertical. Lidar accurately observes the cloud-base height and phase, but attenuates quickly in the vertical. Thus, an optimal combination of these instruments is used to produce a comprehensive cloud properties dataset.

While the algorithm described here has been applied to multiple Arctic locations, it is demonstrated here using 2 yr of observations from the U.S. Department of Energy Atmospheric Radiation Measurement (ARM) Program's North Slope of Alaska (NSA; Stamnes et al. 1999) site in Barrow, Alaska (71°19.38′N, 156°36.54′W). Based on these observations, average annual cycles of cloud microphysical properties at Barrow are presented. These results are evaluated within the context of radiative closure experiments and are compared to a similar microphysics data product from the ARM Program to assess the impact of specific retrieval components on cloud radiative properties.

2. Algorithm design

The cloud property retrieval system described here, termed ShupeTurner (hereinafter ST), is largely based on existing methods that were designed to be conditionally applied to individual cloud scenes. Each method utilizes a unique set of instruments and measurements. The distinctive aspect of this system is the manner in which the strengths of individual measurements and methods are combined within the same framework to provide an estimate of cloud properties in all conditions. The system utilizes the measurements listed in Table 1. While only the specific instruments that are available at the NSA site have been listed, similar instruments that provide the same type of measurements can be substituted for application of this system at other Arctic sites. The retrieval system structure is outlined by the flowchart in Fig. 1, which indicates the interconnections between system elements and the stages at which data are input into the system. The individual methods that are used are outlined in Table 2 and are described here briefly.

a. Atmospheric state

Initially, a series of algorithms is applied to produce needed atmospheric parameters from raw measurements. The microwave radiometer retrieval (MWRRET; Turner et al. 2007) is run operationally by the ARM program and consists of a multichannel microwave retrieval that is constrained by information from atmospheric radiosoundings and surface meteorological measurements to produce initial liquid water path (LWP) and precipitable water vapor (PWV) estimates. To characterize the atmospheric state continuously, the ARM Program also

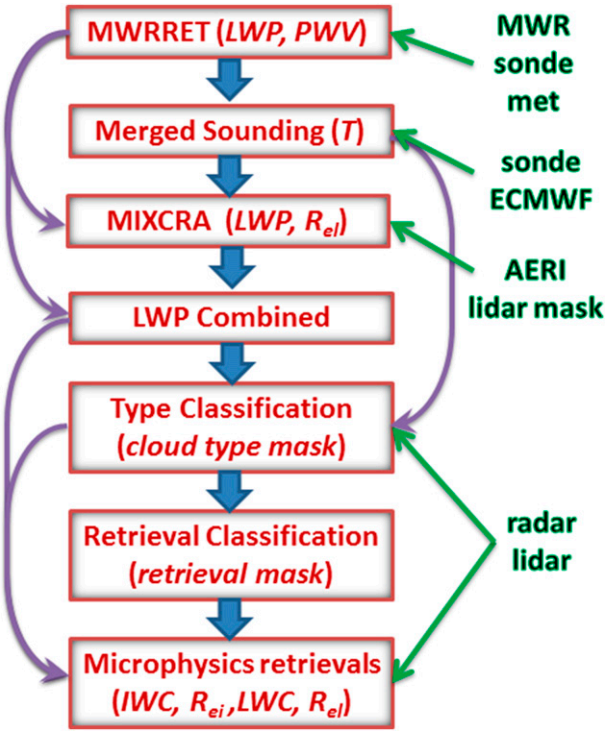

FIG. 1. The ST microphysics retrieval flowchart showing input measurement streams in green and individual algorithm elements in red boxes.

operationally produces a "merged sounding" product that is based heavily on temporally interpolated, twice-daily radiosonde measurements. Background information from the European Centre for Medium-Range Weather Forecasts operational model contributes to this product above the height of radiosondes and helps to fill large gaps between soundings. Moisture profiles in this product are constrained by the MWRRET PWV. These thermodynamic profiles are combined with infrared radiances and a lidar cloud mask using the Mixed-Phase Cloud Retrieval Algorithm (MIXCRA; Turner 2005) to yield an improved estimate of LWP that is optimally combined with the MWRRET LWP product. Turner (2007) has highlighted the benefits of combining microwave and infrared measurements for LWP retrievals; at low LWPs the infrared measurements are most sensitive to liquid water and microwave retrievals are highly uncertain, while at higher LWPs the infrared measurements become saturated but the microwave retrievals are more reliable. Having two perspectives on LWP also allows for LWP information even if one set of measurements is missing for a given time period.

b. *Cloud-type classification*

Once robust atmospheric state parameters are available, they are combined with cloud radar, lidar, and ceilometer measurements to make a vertical cloud-type classification (Shupe 2007) that distinguishes cloud volumes by phase and hydrometeor types. Type classification is important and necessary to ensure that the correct microphysical retrieval methods are applied to the appropriate clouds. The classification is a threshold-based, multisensor algorithm that exploits phase-specific signatures to classify cloud parcels as ice, liquid, mixed phase, drizzle, rain, or snow. While this classification can be applied to cloud observations in other locations, it has been specifically tuned for optimal operation in the

TABLE 2. The ST retrieval framework elements. For cases in which multiple conditions are met for a given retrieval, the method farthest down the table is utilized. The definitions of optically thick and optically thin are based on saturation of the AERI signal; the distinction occurs at a visible optical depth of ~6. The climatological R_{el} is 8 μm. Conditions noted with an asterisk are not applied in the dataset evaluated here.

Retrieval element	Conditions	Measurements	Reference
Type classification	All	Z_e, V_D, W_D, δ, β, $T(z)$, LWP, and z_{base}	Shupe (2007)
IWC, IWP, and R_{ei}	All	Z_e	Generic empirical; Shupe et al. (2005)
	Single-layer cirrus, unobstructed*	Z_e and infrared radiances	Matrosov (1999)
	Optically thin, ice only*	Infrared radiances	Turner (2005)
LWP	All	Microwave T_B and infrared radiances	Turner et al. (2007); Turner (2007)
LWC and R_{el}	Liquid-only clouds (no mixed phase), optically thick	Z_e and LWP	Frisch et al. (1995)
	Liquid-only clouds (no mixed phase), optically thin	Z_e, LWP, and infrared radiances	LWC; Frisch et al. (1995) R_{el}; Turner (2005)
	Liquid mixed with ice and/or drizzle, optically thick	z_{base}, z_{top}, LWP, and $T(z)$	LWC; adiabatic with LWP constraint R_{el}; climatology
	Liquid mixed with ice and/or drizzle, optically thin	z_{base}, z_{top}, LWP, $T(z)$, and infrared radiances	LWC; adiabatic with LWP constraint R_{el}; Turner (2005)

Arctic where deeper convection is limited. The classification identifies the hydrometeor type within individual time–height "pixels" of observations that have been interpolated to 1 min by 50–100 m. For example, if both liquid and solid hydrometeors exist within a pixel, it is classified as mixed-phase. Similarly, an ice classification indicates that only ice particles exist within the pixel. The distinction between cloud and precipitation hydrometeors is generally based on radar reflectivity and mean Doppler velocity thresholds. This distinction is fairly clear between liquid cloud droplets, drizzle, and rain. On the other hand, the division between ice cloud and snow is arbitrary and does not necessarily reflect a true microphysical distinction.

c. *Scene classification*

In addition to cloud type, the vertical distribution of types, availability of measurements, and limitations of retrieval algorithms determine the actual cloud microphysical retrievals that can be applied to a given cloud parcel. The scene classification is where important decisions are made regarding the application of conditional retrievals (listed in Table 2). For example, retrievals based on infrared measurements can be applied to a cloud scene with an LWP of less than $\sim 60\,\mathrm{g\,m^{-2}}$ but not to a thicker cloud scene. Also, an ice cloud retrieval based on radar and infrared radiances can only be used if there is not a lower, intervening cloud layer.

d. *Microphysics retrievals*

With a scene classification in place, individual, conditional cloud retrievals are implemented (Table 2). Cloud ice properties such as ice water content (IWC), its vertical integral that yields the ice water path (IWP), and ice particle characteristic size (effective radius, R_{ei}) are derived from cloud radar measurements. These retrievals exploit the dominant radar return from large ice crystals even if liquid water droplets are also present (Shupe et al. 2004). Ice and snow retrievals are based on empirical radar-reflectivity power-law relationships (e.g., Sassen 1987; Atlas et al. 1995). Retrieval coefficients are derived for Arctic-specific conditions, with seasonal variability determined from infrared measurements (Shupe et al. 2005). Multisensor ice retrieval algorithms can also be implemented that use infrared radiances or optical depths (e.g., Turner 2005) to constrain radar-reflectivity-based retrievals (Matrosov 1999). While these multisensor retrievals may improve the instantaneous retrieval quality relative to radar-only retrievals, it is not clear that they improve the statistical results when applied to long-period datasets and they are typically applicable to only a small fraction of observed ice clouds (Shupe et al. 2005). Thus, multisensor ice cloud retrievals have not been implemented in the dataset presented here. Based on statistical intercomparisons of multiple retrieval methods and limited comparisons with aircraft measurements, the uncertainties of these ice retrievals are expected to be up to 46% for particle characteristic size and a factor of 2 for IWC (Shupe et al. 2005). Ice retrievals cannot be performed if radar data are not available.

As opposed to the solid phase, where the radar signal is strongly sensitive to ice crystals in most conditions, no single instrument is particularly well suited for observing cloud liquid water in all conditions. Thus, while some instances of cloud liquid water can be microphysically characterized using a synergy of measurements and methods, other cases are hard to characterize. There are four retrieval situations within which liquid water occurs: liquid-water-only clouds versus those that also contain larger hydrometeors such as ice crystals (i.e., mixed phase) or drizzle drops, and either of these states wherein the cloud scene is optically thick or optically thin (the distinction between these is a visible optical depth of ~ 6). As described above, the combination of microwave and infrared measurements provides a robust estimate of LWP over the full range of conditions (Turner 2007). The LWP is used as a constraint by which the cloud water is vertically distributed in liquid-only clouds using radar-reflectivity profiles according to the Frisch et al. (1995) liquid water content (LWC) retrieval. For cases that additionally contain larger hydrometeors, radar measurements are typically dominated by the large particles and provide limited information on the liquid droplets. In these cases, a scaled-adiabatic assumption is used whereby an adiabatic liquid water profile is computed using radar- and/or lidar-observed cloud boundaries and radiosonde-based thermodynamic profiles. The liquid water profile is linearly scaled to match the LWP. While this retrieval may not capture the vertical profile shape of liquid water, particularly in subadiabatic conditions, it does specify an appropriate amount of liquid within the appropriate layers. Thus, while depending on conditions, the uncertainty in derived LWPs can range from 5 to $25\,\mathrm{g\,m^{-2}}$, individual LWC estimates at a given height have even a larger relative uncertainty.

Regardless of the presence or absence of larger hydrometeors, cloud droplet effective radius R_{el} can be derived in optically thin conditions when portions of the infrared spectrum are semitransparent (Turner 2005). Comparisons of infrared-based R_{el} retrievals to aircraft in situ observations suggest a mean retrieval bias of less than $1\,\mu\mathrm{m}$ (Turner 2007; Vogelmann et al. 2012). As cloud optical thickness increases, the cloud becomes opaque at infrared frequencies, which no longer contain

information on droplet size. For these optically thick cases, if there are no large hydrometeors present, the Frisch et al. (1995) method, which assumes a constant droplet number concentration with height, yields an R_{el} that is self-consistent with the LWC. These retrievals have uncertainties of up to 32% (Shupe et al. 2005). Finally, for optically thick cases with large hydrometeors (mixed-phase or drizzling clouds), no measurements are available to readily derive R_{el}. In these cases, a climatological value of 8 μm is assumed based on previous Arctic liquid cloud results (Turner 2005; Shupe et al. 2005).

For the results presented here, liquid-phase precipitation (drizzle or rain), which occurs periodically in summer, has not been characterized microphysically and is not included in the statistics. This limitation is in large part due to difficulties in characterizing LWP under liquid precipitation conditions. MWR measurements are most appropriate for quantifying the LWP for typically thick precipitating clouds, but liquid precipitation accumulates on and/or wets the MWR so that robust retrievals are not possible. Future improvements to the algorithm may incorporate radar attenuation-based retrievals in liquid precipitation (Matrosov et al. 2006).

While the uncertainties associated with individual retrieval methods have been summarized above and are discussed in detail within the cited references, it is unclear how these uncertainties combine within the retrieval framework. The aggregate uncertainty will be affected in two significant, and competing, manners. First, the fact that some retrieval is applied to all observed cloud conditions suggests that there may be circumstances in which the specific retrievals are pushed beyond their limits of applicability. The cloud-type and scene classifications are designed to minimize this issue, but generally lack independent sources for evaluation. On the other hand, the strength of this system is that it combines a broad set of instruments, measurements, and retrieval methods to observe and quantify cloud properties over a wide range of conditions. While uncertainties for this retrieval suite, and others, have been examined by Zhao et al. (2012), no attempt is made here to determine an overall uncertainty for the system; indeed, there are extremely limited datasets to use for this purpose. Instead, the retrieved microphysics results are evaluated in aggregate through radiative closure experiments outlined in section 5.

3. Example results

A case study from 24 October 2004 is used to demonstrate the microphysics retrieval system. On this day a near-surface low pressure system moved into central Alaska from eastern Siberia, with east-northeasterly winds below 3-km altitude impinging on Barrow from the open water of the adjacent Arctic Ocean. Winds above 3 km were primarily from the opposite, west-southwesterly, direction. Many of the NSA site measurements on this day are illustrated in Fig. 2, while retrieved cloud properties are shown in Fig. 3. Selected radar and lidar measurements show a two-layer cloud system, with each layer advecting from distinct directions. The lower layer (<1 km) was a typical Arctic stratiform cloud exhibiting a layer of high lidar backscatter and low depolarization ratio indicative of cloud liquid, with periodic high depolarization ratio and radar reflectivity suggesting precipitating ice crystals. Cloud-layer temperatures, derived from radiosondes, were approximately from −8° to −5°C, which is a common range for Arctic mixed-phase stratiform clouds. Wide radar spectral widths also indicated higher turbulence within this layer, which is typically driven by cloud-top radiative cooling. The upper, cirrus cloud (>3 km) contained signatures of ice, including high lidar depolarization ratios (when lidar measurements could observe above the lower cloud), low radar spectral widths, and temperatures down to about −30°C. The cloud-type classification algorithm captured this general structure (Fig. 3a).

Microphysics retrievals illustrate the evolution of both ice and liquid water in this scene over time. The upper ice cloud contained a background field of ice crystals with an IWP of 20 g m^{-2} or less and periodic pulses of

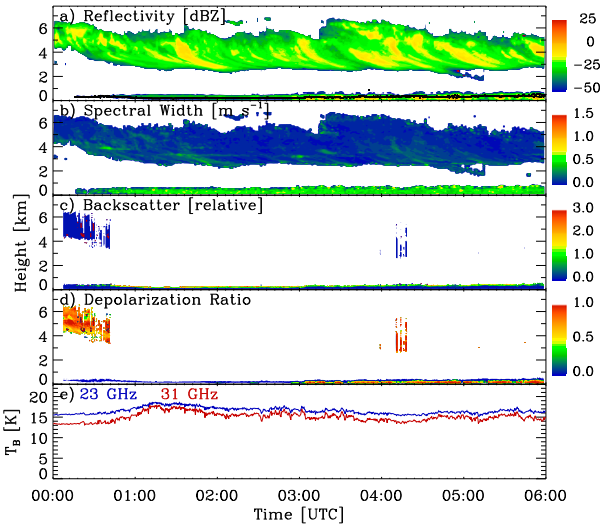

FIG. 2. Measurements from the ARM NSA site on 24 Oct 2004 of (a) radar reflectivity (dBZ from −50 to 25), (b) radar Doppler spectral width (m s^{-1} from 0.0 to 1.5), (c) lidar backscatter (relative from 0.0 to 3.0), (d) lidar depolarization ratio (from 0.0 to 1.0), and (e) microwave brightness temperatures (K from 0 to 20) at 23 (blue) and 31 GHz (red). In (a)–(d), white represents clear sky and/or no measurements for the given instrument. Attenuation of the lidar signal is apparent in (c) and (d).

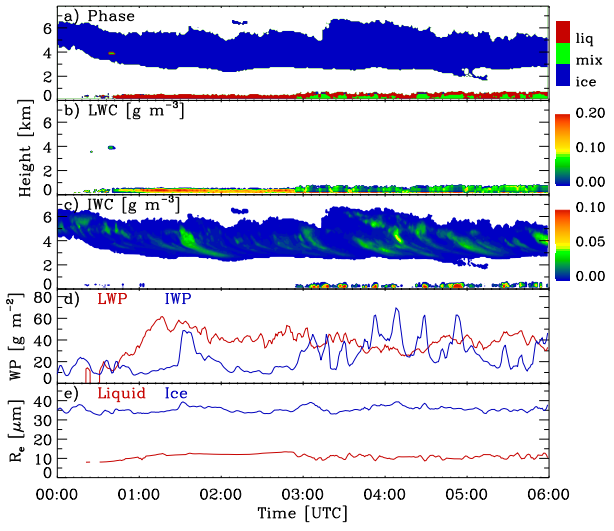

FIG. 3. Retrieved cloud properties from the ARM NSA site on 24 Oct 2004 of (a) cloud phase (ice, mix, or liquid), (b) LWC (g m^{-3} from 0.00 to 0.20), (c) IWC (g m^{-3} from 0.00 to 0.10), (d) LWP (g m^{-2} from 0 to 80) (red) and IWP (blue), and (e) layer-average hydrometeor effective radius (μm from 0 to 40) for liquid (red) and ice (blue).

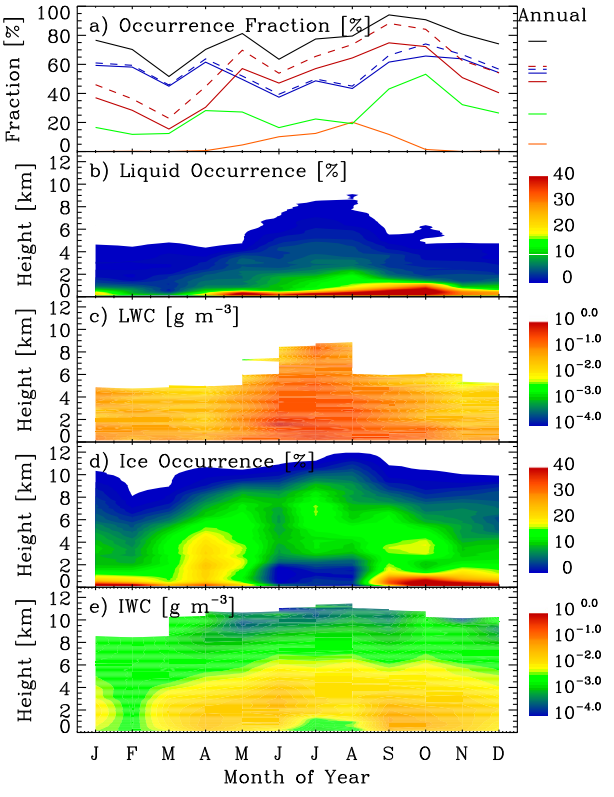

FIG. 4. Annual cycle results characterizing monthly (a) cloud occurrence fraction for different cloud types. The curves represent all clouds (black), all-liquid clouds (red), all-ice clouds (blue), mixed-phase clouds (green), liquid precipitation (orange), liquid in any form (dashed red), and ice in any form (dashed blue). Note that all-ice and all-liquid clouds can occur at the same time, albeit in distinct vertical layers. Annual averages are given to the right. (b)–(e) Vertical monthly distribution of liquid occurrence in any type of cloud (% from 0 to 40), mean LWC when clouds are present (g m^{-3} from $10^{-4.0}$ to $10^{0.0}$), vertical distribution of ice occurrence in any type of cloud (% from 0 to 40), and mean IWC when clouds are present (g m^{-3} from $10^{-4.0}$ to $10^{0.0}$), respectively.

enhanced ice formation. Particle effective radii were near 35 μm with slightly larger sizes during periods with increased ice mass. The lower cloud initially contained only liquid water, forming toward the beginning of the case with LWP growing to 60 g m^{-2} over the first hour. Toward the second half of the case, the LWP decreased to about 40 g m^{-2} while the layer started to precipitate ice. Coincident with this transition, the R_{el} slightly decreased to about 10 μm. Enhanced IWP variability at this time coincided, in part, with periodic pulses of ice from the lower, mixed-phase cloud.

4. Annual cycle results

The cloud retrieval system was applied to NSA observations from the 2-yr period of 1 March 2004–28 February 2006. This date range was chosen because of consistent instrument operations and data quality. It was also chosen as a representative test period for comparisons with other retrieval products (e.g., Zhao et al. 2012) and for conducting radiative closure analyses that are described below. This complete 2-yr cycle also provides a statistical representation of the clouds that occur over Barrow. Thus, an overview of basic retrieval results is summarized here as a first annual cycle assessment of cloud microphysical properties at Barrow. Future research will expand this analysis to longer time periods and compare these results to those from other Arctic cloud observatories.

Monthly fractional occurrence of different cloud types is given in Fig. 4a. Clouds occur ~75% of the time, with an autumn maximum above 90% and a March minimum below 60%. Annually, ice-only clouds occur more than half the time, and slightly less often in summer than during the other months. Liquid-only clouds are most frequent in summer and autumn months, but occur to some extent in all seasons. Mixed-phase cloud volumes occur 25% of the time with transition season maxima. Statistics of the occurrence of liquid or ice in any cloud type are similar to, but somewhat higher than, their single-phase counterparts because of the addition of mixed-phase clouds. Annually, both cloud ice and liquid water occur about 57%–58% of the time. While this result might be expected for cloud ice, the high frequency of liquid water occurrence is notable. This is

particularly true for the winter season when cloud-level temperatures often reach well below −20°C. Even in the coldest month of the year (March), cloud liquid water still occurs 25% of the time. Liquid-phase precipitation, however, is limited to May–September and only 5% of the time annually.

These cloud-type occurrence results are similar to those presented by Shupe (2011) in a study that compared cloud-type occurrence at three Arctic locations. However, here the classification was performed for individual atmospheric volumes (time–height pixels), while in Shupe (2011) this same classification was initially applied and then modified such that ice falling from liquid or mixed-phase layers was reclassified as part of a mixed-phase cloud system. The intention in that paper was to distinguish the formation mechanisms of cloud parcels, while here it is to distinguish the occurrence of phase in order to apply the appropriate microphysics retrieval algorithms.

The vertical distributions of liquid and ice occurrence (Figs. 4b,d) are both influenced by the vertical and annual variability of atmospheric temperature. Liquid water is always more frequent closer to the surface, where temperatures are typically warmer. Similarly, liquid more often extends higher into the atmosphere in summer, occurring on occasion as high as 8 km (e.g., Shupe 2011). The prevalence of low-level liquid-water-containing clouds in the Arctic has been noted often (Herman and Goody 1976; Curry 1986; Intrieri et al. 2002; Shupe et al. 2005). Cloud ice is also frequently observed at low levels, but moves to higher altitudes in summer when near-surface temperatures often reach above the melting point. The near-surface ice maximum observed in nonsummer months is due in large part to ice crystals produced by liquid and mixed-phase clouds, but in the winter and spring much of this near-surface ice is also diamond dust forming without liquid water present.

A comparison of condensed water content and integrated water path for cloud liquid and ice, when clouds are present, provides interesting insight into seasonal cloud processes and also shows important dependencies on temperature (Figs. 4c, 4e, and 5a). Liquid water is typically present at higher masses than ice, both in an integrated sense and when vertically distributed. In late winter and early spring, when temperatures are coldest, the liquid diminishes and the difference becomes smallest. Ice tends to have more vertical variability; IWC decreases with height except right near the surface in summer. LWC shows relatively little vertical variability. Seasonally, there is more condensed liquid water mass in June–August than during the rest of the year when the mean LWC does not vary by much. Ice shows weak maxima in the transition seasons, corresponding to

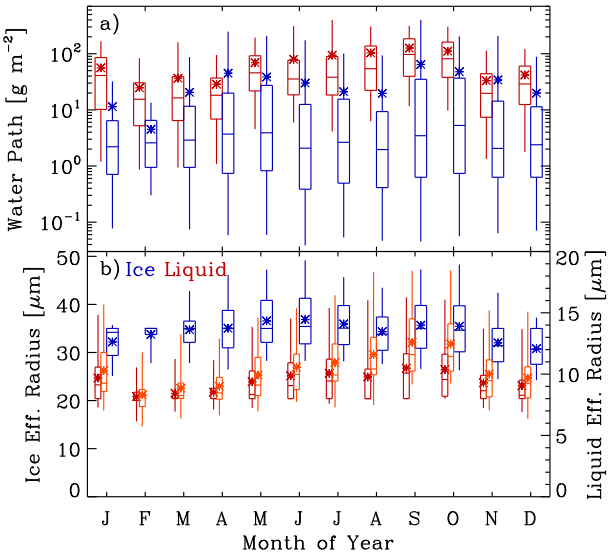

FIG. 5. Annual cycles of cloud properties for liquid (red) and ice (blue) hydrometeor populations in any type of cloud, including (a) integrated condensed water paths and (b) layer-averaged effective radius for ice and liquid clouds. Box-and-whisker diagrams include the 5th, 25th, 50th, 75th, and 95th percentiles with the mean as a symbol. Orange plots in (b) include statistics for only those points for which a value is retrieved (i.e., excluding points at which the climatological value is assumed).

periods where relatively warm, subfreezing temperatures exist near the surface and mixed-phase processes are prevalent. It is important to note that the occurrence fractions and mean condensed water contents for liquid and ice do not mimic each other exactly. Additionally, the fractional occurrence of clouds, which is driven largely by cloud persistence (e.g., Shupe 2011), is not necessarily linked to the amount of mass they possess. For example, midlevel liquid clouds in summer have high LWC, but do not occur frequently. On the other hand, in some seasons the low-level clouds that are known to be quite persistent do not contain any more mass than clouds at other heights.

Particle characteristic sizes also provide insight into annually varying processes (Fig. 5b). For optically thick mixed-phase or multilayered clouds, there is little observational information from the instruments employed here on liquid droplet sizes; for such cases an R_{el} of 8 μm is assumed. This value may influence the statistics; thus, layer-averaged R_{el} statistics have been derived for both the full dataset and the subset for which R_{el} was actually computed (75% of the time). For both sets, an annual cycle in droplet size is apparent, with minimum sizes in late winter–early spring and a 4–5-μm increase toward summer and late fall. The retrieved summer sizes are often larger than the assumed value of 8 μm, although it is not clear if droplet sizes in thick mixed-phase clouds

would be larger or smaller than for other cloud types. This same annual cycle has been previously observed for Arctic liquid water clouds in multiple locations (Turner 2005; Shupe et al. 2005; Dong and Mace 2003; Cox et al. 2014) and is likely related to the spring maximum in aerosol concentrations associated with Arctic haze and advection from lower latitudes (e.g., Barrie and Hoff 1985). For ice particle characteristic size there is a broad maximum through summer and minimum in midwinter. The fact that the spring increase in ice crystal sizes starts at least a month ahead of the transition in liquid droplet sizes suggests that ice is less influenced by the seasonal changes in background aerosol populations.

5. Evaluation

The Barrow cloud microphysics results are evaluated here within the context of a radiative closure analysis. This analysis entails including the derived microphysical properties in atmospheric radiative transfer calculations to estimate broadband radiative fluxes at the surface and top of the atmosphere (TOA) that are subsequently compared with ground- and satellite-based measurements, respectively. This type of radiation comparison is important in that it reveals the cumulative, radiatively significant impacts of uncertainties in the derived cloud microphysical properties. Other forms of evaluation are also possible using intercomparisons of different methods and comparisons with aircraft observations (e.g., Turner 2005; Shupe et al. 2005, 2006; Turner and Eloranta 2008; Vogelmann et al. 2012; Zhao et al. 2012), although these are not covered here.

The radiative transfer framework employed here is called the Broadband Heating Rate Profiles (BBHRP; McFarlane et al. 2015) project, which is a major initiative within the ARM program. It is based on the RRTM radiation code (Mlawer et al. 1997; Clough et al. 2005) for both longwave (LW) and shortwave (SW) radiation. The ''merged sounding'' product described in section 2 is used to characterize atmospheric temperature and moisture profiles. Trace gas species other than water vapor are from the subarctic summer or winter standard atmospheres, wherein the former is used for June–September and the latter for other months. No aerosol properties are included in the radiative transfer calculations. Surface temperature is derived from downlooking pyrgeometer observations, wherein a surface emissivity of 1 is assumed; this same assumption is used in the RRTM calculations. Surface albedo is derived using the ratio of upwelling and downwelling SW observations from pyranometers at the NSA site. These surface broadband radiative flux measurements are used for comparison with calculated surface fluxes. TOA fluxes are provided by cross-track observations (~20-km spatial resolution at nadir) from the Clouds and the Earth's Radiant Energy System (CERES; Wielicki et al. 1998) on board the *Aqua* and *Terra* satellites following Loeb et al. (2005, 2007). CERES fluxes are subsected from 70.8° to 71.8°N, 156.3° to 157.3°W, and only those data within 20 km of Barrow at less than a 40° viewing angle are used in the analyses.

Radiative closure is only considered for downwelling surface fluxes and upwelling TOA fluxes because their counterparts in the opposite directions have little to do with clouds. Rather, these are to first order dominated by properties that are simply specified for the radiative transfer model such as surface temperature, albedo, sun angle, etc. All closure comparisons are made using the average computed and observed fluxes over 10-min windows every 30 min, to minimize the impact of instrument field-of-view differences and small-scale heterogeneity in the conditions. The flux calculations themselves were performed every 1 min, before averaging over 10 min. The layering used in the radiative transfer modeling was at the vertical resolution of the cloud property dataset.

The BBHRP framework was designed to perform radiative closure exercises of this type to evaluate cloud retrieval algorithms (e.g., Turner 2007). The metrics used for this evaluation are the median difference and interquartile range (IQR) of differences between measured and calculated fluxes. The first of these provides some indication of bias, and the second offers insight into variability. Often the variability is a more important metric when comparing different datasets because there can be many unrelated sources of error that can contribute to systematic biases. While a significant effort has been made to ensure the accuracy of the BBHRP system, there are still radiative residuals that are independent of the cloud properties; these could be related to atmospheric aerosols or trace gases, measurement geometry, and others. Thus, it is important to also evaluate the radiative closure under clear-sky conditions to have a reasonable assessment of the cloudy-sky closure analysis.

a. Radiative closure analysis

To develop an understanding of the cloud microphysics retrieval and how different subcomponents perform and/or where the sources of important uncertainty reside, radiative closure is examined for a variety of conditions that are subsets of the full dataset. These subsets include the important distinction between clear skies and cloudy skies. Within the cloudy skies, subsets are examined of single-layer liquid, mixed-phase, and ice clouds to isolate performance in these

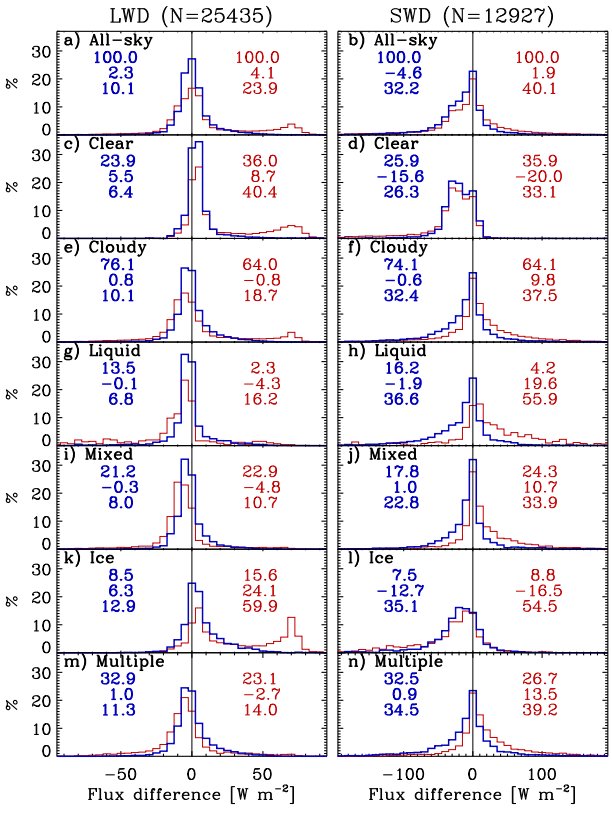

FIG. 6. Distributions of radiative closure flux differences (observations − calculations) of surface downwelling (left) LW and (right) SW fluxes for all sky, clear sky, cloudy sky, single-layer liquid clouds, single-layer mixed-phase clouds, single-layer ice clouds, and multilayer clouds. Results using ST microphysics are in blue and using MB are in red. Each distribution sums to 100%. Each panel also includes the percentage of the total dataset that resides within that subclass (%), the median difference ($W m^{-2}$), and the interquartile range ($W m^{-2}$). Total number of points is given at the top of each column of plots.

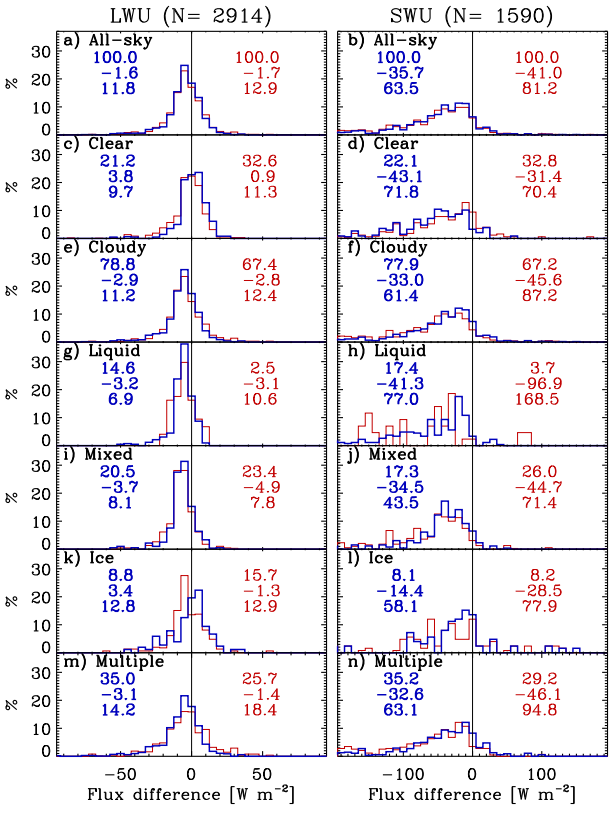

FIG. 7. As in Fig. 6, but for TOA upwelling (left) LW and (right) SW radiative closure flux differences (observations − calculations).

simplified conditions, as well as multilayer cloud scenes for completeness. Finally, the all-sky radiative closure is assessed to demonstrate the aggregate performance of the full cloud microphysics plus radiative transfer model system.

Clear skies occur ~25% of the time over Barrow. Surface radiative closure results during these times (Fig. 6c) show a downwelling LW bias of 5.5 $W m^{-2}$ with an IQR of 6.4 $W m^{-2}$, and a distribution mode near 0 $W m^{-2}$. For the smaller subset of clear-sky downwelling SW cases the results are −15.6 and 26.3 $W m^{-2}$, respectively, with a distribution that is skewed toward negative differences (Fig. 6d). This distribution appears to be bimodal, with the primary mode at −30 $W m^{-2}$. Together these results indicate that the BBHRP system underestimates downwelling LW and overestimates downwelling SW radiation at the surface under clear skies, consistent with an atmosphere that is too optically thin. Two potential sources that could contribute to this bias include the lack of aerosols in the radiative transfer calculations, and the contamination from off-zenith clouds that are in the hemispheric radiometer view while it is clear overhead or the instruments missing thin clouds overhead altogether.

The TOA dataset (Fig. 7) is smaller than the surface dataset because satellite radiative flux estimates can be made less frequently. For this subset, clear skies occur ~22% of the time. Calculated upwelling LW fluxes are reasonably well represented (Fig. 7c), being biased low by 3.8 $W m^{-2}$ with an IQR that is 50% larger than the surface LW counterpart. The BBHRP system is too reflective at the TOA with high variability in upwelling SW relative to the observations (Fig. 7d); the bias is −43.1 $W m^{-2}$ and the IQR is 71.8 $W m^{-2}$. Relative to surface closure, wider IQRs are expected for TOA closure because of challenges in comparing satellite footprints with column radiative transfer calculations. The LW bias suggests that the modeled surface temperature may be slightly low or that there is a bias introduced by the large satellite footprint, which can include land, ocean, or both. Similarly, the TOA SW bias is likely due to both biases in downwelling surface SW and differences in surface albedo wherein the effective albedo for satellite observations is lower

than for NSA radiometers because of the inclusion of summertime open ocean adjacent to Barrow. The large SW IQR may also be due to spatial inhomogeneities in the surface properties.

These clear-sky values indicate important uncertainties caused by the modeling framework, assumptions being used, and difficulties in comparing column calculations with observational data that include a spatial component. As a result of the significant clear-sky biases, and because it is not apparent how these biases manifest under cloudy skies, bias is considered to be of second-order evaluative importance here. A more important metric is the IQR, which quantifies the variability in a given comparison. Using these metrics in comparison with clear-sky results, the radiative closure for cloudy scenes is evaluated.

1) SURFACE DOWNWELLING LW FLUX

It is noteworthy that, except for single-layer ice clouds, all cloud subsets show smaller surface LW biases (Figs. 6e,g,i,k,m) than under clear skies (Fig. 6c). For clouds that contain liquid water (Figs. 6g,i), biases are less than $1\,\mathrm{W\,m^{-2}}$. Thus, the conditions leading to clear-sky bias may actually be minimized under cloudy skies. On the other hand, IQR statistics exhibit a 60% increase relative to clear skies. Of the different cloud types, single-layer liquid and mixed-phase clouds (i.e., clouds with one liquid layer) have the smallest IQRs; these are only 20% larger than for clear skies. Ice and multilayer cloud scenes (Figs. 6k,m) are more variable and include more extreme values. Ice clouds show a tail toward large positive differences, where the calculations are strongly underestimated and cloud optical thickness may be underestimated.

2) SURFACE DOWNWELLING SW FLUX

The magnitudes of cloudy-sky downwelling SW closure biases (Figs. 6f,h,j,l,n) are again smaller than those for clear sky (Fig. 6d), in some cases substantially so. Distributions of flux differences all have modal values at $0\,\mathrm{W\,m^{-2}}$, except for single-layer ice clouds with a mode at $-20\,\mathrm{W\,m^{-2}}$. Apart from single-layer mixed-phase clouds, all other cloud types have larger IQRs than clear skies, generally exceeding $30\,\mathrm{W\,m^{-2}}$. The cloudy-sky IQR is 25% larger than for clear sky. All cloudy-sky subsets have long tails toward negative flux differences, indicating an overestimation of downwelling SW flux and thus an underestimation of cloud optical thickness.

3) TOA UPWELLING LW FLUX

Similar to the surface LW, all cloudy TOA LW biases (Figs. 7e,g,i,k,m) are smaller than for clear skies (Fig. 7c), but some have the opposite sign. The IQR for single-layer liquid-containing clouds is smaller than for clear skies, while those for ice and multilayered cloud scenes are larger by as much as 46%.

4) TOA UPWELLING SW FLUX

SW radiative closure at the TOA is by far the worst of any of the terms, with all cloudy subsets (Figs. 7f,h,j,l,n) having broad distributions of differences with long negative tails (i.e., calculations are too reflective) and few positive points. Nonetheless, except for the single-layer liquid cloud IQR, all cloudy-sky biases and IQRs are smaller than those for clear skies. This again suggests that clouds mitigate some issues that contribute to large clear-sky biases, such as the influence of surface albedo differences. Ice clouds have a smaller bias than any other cloud type, with a primary mode that is only slightly negative. However, there are some cases with large flux differences, such that the IQR is still relatively large. The smaller bias suggests that the reflectivity of ice clouds may be somewhat better than for other types, perhaps because of their higher altitude.

It is interesting to note that in surface LW, surface SW, and TOA LW cases, the distributions of flux differences for single-layer ice clouds are similar to those for clear skies, while those for other cloudy skies are distinct and have relatively smaller biases. For example, both ice and clear-sky scenes are strongly positively biased in surface LW but strongly negatively biased in surface SW. These results suggest that modeled clear and ice cloud atmospheres are too optically thin relative to the observed downwelling fluxes, while liquid-containing clouds are approximately correct. This could be caused by instrument sensitivity limitations leading to the incorrect distinction of clear versus thin ice cloud conditions or by failing to identify when very small amounts of liquid water are present. TOA results are consistent with ice and clear-sky scenes being slightly too cold and liquid-containing scenes being slightly too warm, resulting from issues in specified surface temperatures or an improper vertical distribution of the cloud properties.

b. Comparisons with Microbase

To help in evaluating individual ST retrieval components, it is insightful to compare these radiative closure results with those from a similar comprehensive cloud product derived operationally by the ARM program. This baseline microphysics product, called Microbase (MB; Dunn et al. 2011), also includes retrieved liquid and ice microphysical properties in all clouds observed above the NSA site and was applied to the same 2-yr dataset. MB employs a simple temperature-based cloud classification and phase partitioning, as well as empirical radar-based cloud retrievals. The LWP is derived using

TABLE 3. Cloud-type classification confusion matrix and radiative closure statistics for all samples with valid downwelling LW flux observations at the surface. Cloud classification by the ST algorithm is labeled along the top row while classification for MB is along the left column. In each box, the top single value represents the number of samples in the box. Other numbers represent the median difference (observations − modeled fluxes) and the interquartile range of differences (in parentheses) for all samples in that box for ST (boldface) and MB (italics).

	ST clear	ST 1layLiq	ST 1layMix	ST 1layIce
MB clear	5321	1430	705	703
	5.7 (6.5)	**−0.8 (9.8)**	**3.2 (13.7)**	**4.4 (10.3)**
	5.6 (6.4)	*65.2 (29.2)*	*60.2 (50.0)*	*7.9 (13.8)*
MB 1layLiq	156	370	23	8
	−0.9 (7.6)	**0.7 (8.0)**	**2.4 (10.8)**	**−0.5 (2.1)**
	−32.1 (46.2)	*−1.1 (8.7)*	*−4.7 (12.3)*	*−29.1 (35.1)*
MB 1layMix	125	1089	3260	185
	3.6 (6.3)	**−0.4 (5.3)**	**−1.5 (7.1)**	**6.6 (13.3)**
	−16.9 (53.3)	*−0.9 (11.5)*	*−6.3 (9.7)*	*−14.6 (33.7)*
MB 1layIce	455	468	1074	1017
	5.7 (4.5)	**1.3 (5.4)**	**1.3 (7.4)**	**8.0 (12.2)**
	5.6 (4.5)	*71.0 (11.3)*	*55.3 (53.4)*	*7.2 (11.6)*

only microwave measurements. The MB microphysical results were used within the same BBHRP framework to derive a radiative closure dataset for comparison to ST. While the two cloud property products have slightly different vertical resolutions, the impact on computed fluxes is less than $1\,W\,m^{-2}$ for all terms.

Comparing radiative closure between two different cloud datasets is complicated by the fact that the different algorithms do not always agree on the cloud-type classification. MB radiative closure statistics, based on its own cloud classification results, are given in Figs. 6 and 7 for direct comparison with ST. A number of key results are readily apparent. First, cloud-type classification statistics are different, and in some categories (e.g., single-layer liquid-only clouds) markedly so. MB identifies more clear sky, more single-layer ice clouds in winter, and fewer single-layer liquid clouds than ST. Almost across the board in every class of data the biases and IQRs are smaller for ST relative to MB, sometimes significantly. For surface LW closure, MB has a second mode at $70\,W\,m^{-2}$ for single-layer ice and clear-sky scenes, both suggesting liquid-water-bearing clouds that went undetected. Additionally, MB has a long tail toward strong negative surface LW residuals for liquid clouds, suggesting that liquid was classified when it did not actually exist. Most of the incorrect liquid classification must be in nonsummer months since these features are much smaller in surface SW results. In general, the primary mode of most MB cloud LW distributions is slightly more negative than for ST. For surface SW, ST has larger tails extending negatively (model overestimating flux) while MB has larger tails extending to the positive side. TOA results between the two techniques are generally similar, with often narrower and less biased distributions for ST closure.

It is apparent that one source of differences in the radiative closure results between ST and MB is the cloud-type classification employed. To explore such differences in more detail, the joint radiative closure dataset is partitioned into subsets based on the cloud classifications of both retrieval packages. This allows for the radiative closure statistics to be computed for cases when the retrievals agree on the classification and those when they do not, as displayed in the confusion matrices in Tables 3 and 4. Only surface radiative closure is discussed here for simplicity. Diagonal table elements describe cases where the methods agree on the cloud classification and offer direct insight into the specific microphysics retrievals that are applied. Off-diagonal elements provide more insight into the effects of cloud classification on radiative closure. Simple counting statistics indicate that there is frequent disagreement on cloud type, especially when ST identifies single-layer liquid water clouds or MB identifies clear skies.

As expected, when both methods agree on clear skies, their closure statistics are nearly identical, only differing slightly because of distinct vertical layering. By and large the closure statistics for agreed-upon classifications are also similar; ice cloud IQRs are slightly smaller for MB, while mixed-phase IQRs are slightly smaller for ST. For liquid-only clouds ST performs better for LW radiation while MB performs better for SW. For SW in particular, the ST cloudy-sky closure results tend to be more distributed like the clear-sky results, indicating that biases may be significantly influenced by the clear-sky model. On the contrary, MB distributions are often biased to the opposite direction as the clear-sky results. However, it is not clear how biases and uncertainties in the clear-sky model impact cloudy-sky calculations.

TABLE 4. As in Table 3, but for downwelling SW radiative closure at the surface.

	ST clear	ST 1layLiq	ST 1layMix	ST 1layIce
MB clear	3022	812	225	236
	−15.6 (26.0)	**1.1 (30.4)**	**−1.0 (18.0)**	**−13.5 (19.9)**
	−15.7 (26.2)	*−70.5 (129.9)*	*−25.2 (69.5)*	*−20.7 (23.0)*
MB 1layLiq	135	351	25	5
	−10.4 (33.2)	**−18.7 (52.3)**	**−14.5 (41.1)**	**−9.3 (19.0)**
	28.7 (88.3)	*16.6 (46.0)*	*31.0 (58.7)*	*7.4 (15.2)*
MB 1layMix	90	782	1654	95
	−13.5 (19.6)	**−0.7 (34.3)**	**1.9 (21.4)**	**−11.4 (44.1)**
	11.0 (54.2)	*10.4 (33.6)*	*11.0 (31.9)*	*13.3 (59.2)*
MB 1layIce	95	87	221	508
	−23.0 (30.8)	**−5.6 (39.9)**	**−3.3 (26.6)**	**−13.2 (40.7)**
	−23.0 (30.4)	*−59.6 (108.9)*	*−29.7 (96.1)*	*−6.6 (37.0)*

Off-diagonal closure statistics for periods when the two methods do not agree on cloud type are particularly revealing. When there are discrepancies, ST closure statistics usually show smaller biases and narrower IQRs, particularly for single-layer, liquid-containing clouds. For LW closure, when ST identifies clouds with liquid water, MB does not identify liquid-water-containing clouds 44% of the time. On the other side, when MB identifies liquid-containing clouds, ST does not only 9% of the time. For the summer SW dataset, the statistics change to 32% and 10%, respectively. Of the cases where MB suggests clear skies, ST identifies liquid water in some form ~25% of the time. Closure results for these various periods show a clear message: When the two methods disagree on liquid water presence, the MB closure statistics degrade substantially while the ST results do not change much relative to other conditions. Together these results indicate that, by using phase signatures from multiple sensors, ST is better at identifying liquid water clouds, particularly in the colder season. These clouds can have strong radiative effects leading to drastic differences relative to liquid-free cloud scenes and thus contributing to the large MB biases.

To further explore this liquid water issue, radiative closure results as a function of LWP are examined (Fig. 8). LWP is an important parameter for Arctic cloud radiative effects and the small quantities that are found there have been difficult to quantify (Shupe et al. 2008). Flux differences are largest for lower LWPs and decrease with increasing LWP. For ST at LWPs greater than about 25 g m^{-2}, closure results converge toward relatively narrow ranges with no median bias. Below this cutoff the IQR increases and there is a small positive bias in LW and negative bias in SW radiative closure. These results suggest that under low liquid water conditions the LWP may be underestimated or other model errors, such as the lack of aerosols, may influence the results. The MB closure results are quite good for the smallest LWP bin (<5 g m^{-2}) but have a growing negative LW bias and positive SW bias as LWP increases. At LWPs greater than ~50 g m^{-2}, MB closure results tend toward a consistent LW underestimate and SW overestimate, with IQRs that are slightly larger than for ST at these LWPs.

These general patterns of flux differences as a function of LWP offer insight into the individual approaches used for deriving that important parameter. The MB approach is statistical microwave-radiometer-based that has an uncertainty of ~25 g m^{-2} (Westwater et al. 2001), which becomes significant for low LWPs. The ST also uses a microwave approach, but combines this with spectral infrared retrievals. Turner (2007) showed that this paired approach, particularly in the Arctic, capitalizes on the ability of infrared measurements at low LWP and microwave measurements at higher LWP to improve the retrieval over a much wider range of conditions. Indeed, this enhanced LWP retrieval appears to have improved radiative closure in both LW and SW for moderate to small LWP conditions.

6. Summary and conclusions

An Arctic cloud microphysics retrieval system is described that is based on measurements from multiple ground-based remote sensors, including cloud radar, depolarization lidar, microwave radiometer, infrared interferometer, and radiosondes. These measurements are incorporated into a retrieval framework that simultaneously determines cloud type and retrieves the vertically resolved water content and particle characteristic size for both cloud liquid and ice throughout the troposphere. The retrieval system is implemented on a 2-yr dataset from Barrow to demonstrate the retrievals, provide insight on the annual variability of cloud microphysics, and serve as a dataset to evaluate the retrieval quality using radiative closure analyses.

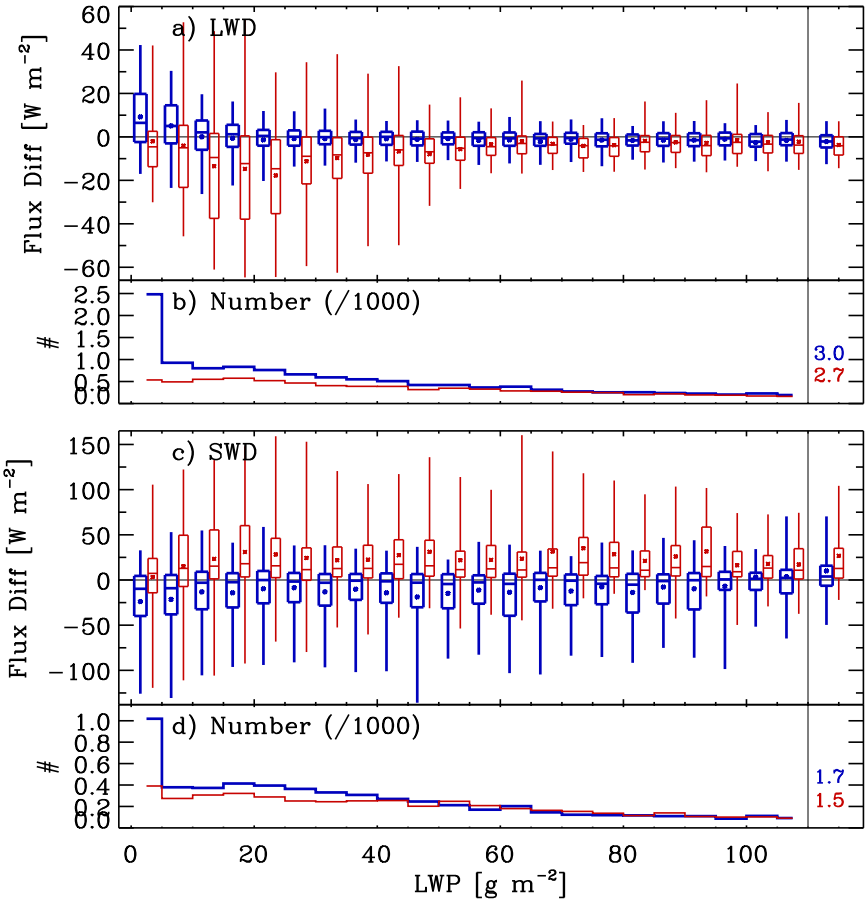

FIG. 8. Statistics of surface radiative closure flux differences (observations − calculations) as a function of LWP for downwelling (a) LW and (c) SW radiation, with the respective numbers per bin in (b) and (d). Results using the ST microphysics are in blue, and those for the MB are in red; both have identical bins but are offset slightly for display purposes. To the right of each panel are the statistics for all cases with LWP > 110 g m^{-2}. Box-and-whisker diagrams include the 5th, 25th, 50th, 75th, and 95th percentiles, with the mean as a symbol.

Monthly microphysics results show that both liquid and ice occur in the column above Barrow about 57% of the time throughout the year, with the former having a maximum occurrence in summer while the later peaks in winter. In spite of cold temperatures, liquid water still occurs at least 25% of the time throughout the winter. While cloud ice can occur throughout the troposphere year round, liquid water is typically at low altitudes but can occur as high as 8 km in the summer. Under cloudy conditions, the mass of liquid in the vertical column is typically larger than the ice mass, with a diminishing difference in winter. Annual variability of liquid droplet size, with a minimum in late winter and maximum in autumn, follows the known variability of aerosol concentrations in the region.

The retrieved cloud microphysical properties were incorporated into the BBHRP radiative transfer system along with other atmospheric parameters to compute radiative fluxes at the surface and TOA for comparison to measured fluxes. Clear-sky radiative closure analyses at the surface suggest that the modeled atmosphere is too optically thin, while TOA analyses reveal the difficulties associated with comparing a narrow vertical column with a satellite footprint. For example, the effective surface albedo for a satellite footprint can include influences from land, ocean, ice, or some combination of these near Barrow, while the assumed surface albedo used for BBHRP modeling is based on land observations. Differences in instrument fields of view, sensitivity limits of ground-based instruments, and the lack of aerosols in radiative transfer modeling likely also contributed to clear-sky biases.

Radiative closure biases were typically reduced under cloudy conditions relative to clear skies, suggesting that clouds mitigate some sources of clear-sky bias and that the retrieved cloud microphysics do not contribute

significantly to radiation biases. Cloudy-sky biases were less than $1\,W\,m^{-2}$ for surface radiation, with flux difference IQRs not more than 50% larger than their clear-sky counterparts. Broadly speaking, the best LW radiative closure at both the surface and TOA was obtained when liquid-containing clouds were present. These are often horizontally extensive stratiform layers that approximate the ''plane parallel'' structure assumed in model calculations. Radiative closure statistics for ice clouds were similar to those for clear-sky periods, both being distinct from the liquid-containing cloud closure statistics.

Comparisons of radiative closure results based on the ST microphysics product presented here with similar results from the simpler MB cloud retrieval system illustrated the impact of key retrieval improvements. For nearly all cloud types, radiative closure statistics for ST were improved over those for MB. However, when the two systems agreed on the cloud-type classification for a given scene, closure results were similar. The largest differences occurred for cases when the two algorithms disagreed on the presence of liquid water, which occurred most frequently in nonsummer months. These results indicate that the ST cloud-type classification, based on phase-specific signatures from multiple sensors, is a significant improvement over the simple temperature-based phase classification employed by the MB. Indeed, temperature alone is a relatively poor constraint on Arctic cloud phase (Shupe et al. 2006), while properly identifying the presence and vertical location of liquid water, especially at highly supercooled temperatures, is critical for radiation. Additionally, the radiative closure comparisons demonstrate that a combined microwave-infrared LWP retrieval shows improved radiative closure for LWP less than $50\,g\,m^{-2}$ compared to microwave-based LWP retrievals.

With radiative flux closure results that compare favorably to clear-sky closure results, the Arctic-specific cloud microphysics retrieval system presented here can be reliably used to explore the temporal and spatial variability of cloud properties across the Arctic. Future work will expand the analysis at Barrow to additional years, and extend to other, similarly instrumented sites in northern Canada, Greenland, and elsewhere. Additionally, such detailed and continuous microphysical characterizations can be used in conjunction with other information on cloud and atmosphere dynamics to study the processes that shape cloud composition and control cloud influences on the Arctic climate system.

Acknowledgments. This research was supported by the Office of Science (BER), U.S. Department of Energy, Grants DE-SC0011918, DE-SC0008830, DE-SC0000991, and DE-FG01-06ER64167. Ground-based datasets were obtained from the ARM data archive (www.archive.arm.gov). Connor Flynn provided the MPL dataset. The CERES satellite data were subsected from the full CERES *Terra* and/or *Aqua* Edition 3A Single Scanner Footprint dataset, obtained from the NASA Langley Research Center Atmospheric Science Data Center (https://eosweb.larc.nasa.gov/order-data) and described online (http://ceres.larc.nasa.gov/documents/DPC/DPC_current/pdfs/DPC_SSF-Ed3_R5V2.pdf).

REFERENCES

Atlas, D., S. Y. Matrosov, A. J. Heymsfield, M.-D. Chou, and D. B. Wolff, 1995: Radar and radiation properties of ice clouds. *J. Appl. Meteor.,* **34,** 2329–2345, doi:10.1175/1520-0450(1995)034<2329:RARPOI>2.0.CO;2.

Barrie, L. A., and R. M. Hoff, 1985: Five years of air chemistry observations in the Canadian Arctic. *Atmos. Environ.,* **19,** 1995–2010, doi:10.1016/0004-6981(85)90108-8.

Clough, S. A., M. W. Shephard, E. J. Mlawer, J. S. Delamere, M. J. Iacono, K. Cady-Pereira, S. Boukabara, and P. D. Brown, 2005: Atmospheric radiative transfer modeling: A summary of the AER codes. *J. Quant. Spectrosc. Radiat. Transfer,* **91,** 233–244, doi:10.1016/j.jqsrt.2004.05.058.

Cox, C. J., D. D. Turner, P. M. Rowe, M. D. Shupe, and V. P. Walden, 2014: Cloud microphysical properties retrieved from downwelling infrared radiance measurements made at Eureka, Nunavut, Canada (2006–09). *J. Appl. Meteor. Climatol,* **53,** 772–791, doi:10.1175/JAMC-D-13-0113.1.

Curry, J. A., 1986: Interactions among turbulence, radiation, and microphysics in Arctic stratus clouds. *J. Atmos. Sci.,* **43,** 90–106, doi:10.1175/1520-0469(1986)043<0090:IATRAM>2.0.CO;2.

de Boer, G., W. Chapman, J. Kay, B. Medeiros, M. D. Shupe, S. Vavrus, and J. Walsh, 2012: A characterization of the present-day Arctic atmosphere in CCSM4. *J. Climate,* **25,** 2676–2695, doi:10.1175/JCLI-D-11-00228.1.

Dong, X., and G. G. Mace, 2003: Arctic stratus cloud properties and radiative forcing at the ARM NSA site. *J. Climate,* **16,** 445–461, doi:10.1175/1520-0442(2003)016<0445:ASCPAR>2.0.CO;2.

——, ——, P. Minnis, W. L. Smith Jr., M. Poellot, R. T. Marchand, and A. D. Rapp, 2002: Comparison of stratus cloud properties deduced from surface, GOES, and aircraft data during the March 2000 ARM Cloud IOP. *J. Atmos. Sci.,* **59,** 3265–3284, doi:10.1175/1520-0469(2002)059<3265:COSCPD>2.0.CO;2.

Dunn, M., K. L. Johnson, and M. P. Jensen, 2011: The Microbase value-added product: A baseline retrieval of cloud microphysical properties. Dept. of Energy Tech. Rep. DOE/SC-ARM/TR-095, 19 pp. + appendixes. [Available online at https://www.arm.gov/publications/tech_reports/doe-sc-arm-tr-095.pdf.]

Frisch, A. S., C. W. Fairall, and J. B. Snider, 1995: Measurements of stratus cloud and drizzle parameters in ASTEX with a Ka-band Doppler radar and a microwave radiometer. *J. Atmos. Sci.,* **52,** 2788–2799, doi:10.1175/1520-0469(1995)052<2788:MOSCAD>2.0.CO;2.

Herman, G., and R. Goody, 1976: Formation and persistence of summertime Arctic stratus clouds. *J. Atmos. Sci.,* **33,** 1537–1553, doi:10.1175/1520-0469(1976)033<1537:FAPOSA>2.0.CO;2.

Illingworth, A. J., and Coauthors, 2007: CloudNet: Continuous evaluations of cloud profiles in seven operational models using

ground-based observations. *Bull. Amer. Meteor. Soc.,* **88,** 883–898, doi:10.1175/BAMS-88-6-883.

Intrieri, J. M., M. D. Shupe, T. Uttal, and B. J. McCarty, 2002: An annual cycle of Arctic cloud characteristics observed by radar and lidar at SHEBA. *J. Geophys. Res.,* **107,** doi:10.1029/2000JC000423.

Klein, S. A., and Coauthors, 2009: Intercomparison of model simulations of mixed-phase clouds observed during the ARM Mixed-Phase Arctic Cloud Experiment. I: Single-layer cloud. *Quart. J. Roy. Meteor. Soc.,* **135,** 979–1002, doi:10.1002/qj.416.

Loeb, N. G., S. Kato, K. Loukachine, and N. Manalo-Smith, 2005: Angular distribution models for top-of-atmosphere radiative flux estimation from the Clouds and the Earth's Radiant Energy System instrument on the *Terra* satellite. Part I: Methodology. *J. Atmos. Oceanic Technol.,* **22,** 338–351, doi:10.1175/JTECH1712.1.

——, ——, ——, ——, and D. R. Doelling, 2007: Angular distribution models for top-of-atmosphere radiative flux estimation from the Clouds and the Earth's Radiant Energy System instrument on the *Terra* satellite. Part II: Validation. *J. Atmos. Oceanic Technol.,* **24,** 564–584, doi:10.1175/JTECH1983.1.

Mace, G. G., Y. Zhang, S. Platnick, M. D. King, P. Minnis, and P. Yang, 2005: Evaluations of cirrus cloud properties derived from MODIS radiances using cloud properties derived from ground-based data collected at the ARM SGP site. *J. Appl. Meteor.,* **44,** 221–240, doi:10.1175/JAM2193.1.

——, S. Benson, and E. Vernon, 2006a: On the relationship between cirrus cloud occurrence and microphysical properties with the large-scale atmospheric state revealed by six years of continuous ground-based cloud radar data. *J. Climate,* **19,** 3257–3278, doi:10.1175/JCLI3786.1.

——, and Coauthors, 2006b: Cloud radiative forcing at the ARM Climate Research Facility: 1. Technique, validation, and comparison to satellite-derived diagnostic quantities. *J. Geophys. Res.,* **111,** D11S90, doi:10.1029/2005JD005921.

Mather, J. H., S. A. McFarlane, M. A. Miller, and K. L. Johnson, 2007: Cloud properties and associated radiative heating rates in the tropical western Pacific. *J. Geophys. Res.,* **112,** D05201, doi:10.1029/2006JD007555.

Matrosov, S. Y., 1999: Retrievals of vertical profiles of ice cloud microphysics from radar and IR measurements using tuned regressions between reflectivity and cloud parameters. *J. Geophys. Res.,* **104,** 16 741–16 753, doi:10.1029/1999JD900244.

——, P. D. May, and M. D. Shupe, 2006: Rainfall profiling using Atmospheric Radiation Measurement Program's vertically pointing 8-mm wavelength radars. *J. Atmos. Oceanic Technol.,* **23,** 1478–1491, doi:10.1175/JTECH1957.1.

McFarlane, S. A., J. H. Mather, and E. J. Mlawer, 2015: ARM's progress on improving atmospheric broadband radiative fluxes and heating rates. *The Atmospheric Radiation Measurement Program: The First 20 Years, Meteor. Monogr.,* Amer. Meteor. Soc., in press.

Mlawer, E. J., S. J. Taubman, P. D. Brown, M. J. Iacono, and S. A. Clough, 1997: RRTM, a validated correlated-*k* model for the longwave. *J. Geophys. Res.,* **102,** 16 663–16 682, doi:10.1029/97JD00237.

Sassen, K., 1987: Ice cloud content from radar reflectivity. *J. Climate Appl. Meteor.,* **26,** 1050–1053, doi:10.1175/1520-0450(1987)026<1050:ICCFRR>2.0.CO;2.

Shupe, M. D., 2007: A ground-based multisensor cloud phase classifier. *Geophys. Res. Lett.,* **34,** L22809, doi:10.1029/2007GL031008.

——, 2011: Clouds at Arctic atmospheric observatories. Part II: Thermodynamic phase characteristics. *J. Appl. Meteor. Climatol.,* **50,** 645–661, doi:10.1175/2010JAMC2468.1.

——, P. Kollias, S. Y. Matrosov, and T. L. Schneider, 2004: Deriving mixed-phase cloud properties from Doppler radar spectra. *J. Atmos. Oceanic Technol.,* **21,** 660–670, doi:10.1175/1520-0426(2004)021<0660:DMCPFD>2.0.CO;2.

——, T. Uttal, and S. Y. Matrosov, 2005: Arctic cloud microphysics retrieved from surface-based remote sensors at SHEBA. *J. Appl. Meteor.,* **44,** 1544–1562, doi:10.1175/JAM2297.1.

——, S. Y. Matrosov, and T. Uttal, 2006: Arctic mixed-phase cloud properties derived from surface-based sensors at SHEBA. *J. Atmos. Sci.,* **63,** 697–711, doi:10.1175/JAS3659.1.

——, and Coauthors, 2008: A focus on mixed-phase clouds: The status of ground-based observational methods. *Bull. Amer. Meteor. Soc.,* **89,** 1549–1562, doi:10.1175/2008BAMS2378.1.

Stamnes, K., R. G. Ellingson, J. A. Curry, J. E. Walsh, and B. D. Zak, 1999: Review of science issues, deployment strategy, and status of the ARM North Slope of Alaska–Adjacent Arctic Ocean climate research site. *J. Climate,* **12,** 46–63, doi:10.1175/1520-0442-12.1.46.

Stubenrauch, C. J., and Coauthors, 2013: Assessment of global cloud datasets from satellites: Project and database initiated by the GEWEX Radiation Panel. *Bull. Amer. Meteor. Soc.,* **94,** 1031–1049, doi:10.1175/BAMS-D-12-00117.1.

Turner, D. D., 2005: Arctic mixed-phase cloud properties from AERI lidar observations: Algorithm and results from SHEBA. *J. Appl. Meteor.,* **44,** 427–444, doi:10.1175/JAM2208.1.

——, 2007: Improved ground-based liquid water path retrievals using a combined infrared and microwave approach. *J. Geophys. Res.,* **112,** D15204, doi:10.1029/2007JD008530.

——, and E. W. Eloranta, 2008: Validating mixed-phase cloud optical depth retrieved from infrared observations with high spectral resolution lidar. *IEEE Geosci. Remote Sens. Lett.,* **5,** 285–288, doi:10.1109/LGRS.2008.915940.

——, S. A. Clough, J. C. Liljegren, E. E. Clothiaux, K. Cady-Pereira, and K. L. Gaustad, 2007: Retrieving liquid water path and precipitable water vapor from the Atmospheric Radiation Measurement (ARM) microwave radiometers. *IEEE Trans. Geosci. Remote Sens.,* **45,** 3680–3690, doi:10.1109/TGRS.2007.903703.

Vogelmann, A. M., and Coauthors, 2012: RACORO extended-term aircraft observations of boundary layer clouds. *Bull. Amer. Meteor. Soc.,* **93,** 861–878, doi:10.1175/BAMS-D-11-00189.1.

Walsh, J. E., W. L. Chapman, and D. H. Portis, 2009: Cloud fraction and radiative fluxes in atmospheric reanalyses. *J. Climate,* **22,** 2316–2334, doi:10.1175/2008JCLI2213.1.

Westwater, E. R., Y. Han, M. D. Shupe, and S. Y. Matrosov, 2001: Analysis of integrated cloud liquid and precipitable water vapor retrievals from microwave radiometers during SHEBA. *J. Geophys. Res.,* **106,** 32 019–32 030, doi:10.1029/2000JD000055.

Wielicki, B. A., and Coauthors, 1998: Clouds and the Earth's Radiant Energy System (CERES): Algorithm overview. *IEEE Trans. Geosci. Remote Sens.,* **36,** 1127–1141, doi:10.1109/36.701020.

Zhao, C., and Coauthors, 2012: Towards understanding of differences in current cloud retrievals of ARM ground-based measurements. *J. Geophys. Res.,* **117,** D10206, doi:10.1029/2011JD016792.